Construction and Building Materials xxx (xxxx) 118356

Contents lists available at ScienceDirect

Construction and Building Materials

journal homepage: http://ees.elsevier.com

Non-linear continuous model for three leaf masonry walls

Claudia Brito de Carvalho Bello *, Giosuè Boscato, Emilio Meroi, Antonella Cecchi

Università IUAV di Venezia, Dorsoduro, 2206, 30123 Venezia, Italy

ARTICLE INFO

Article history:
Received 17 July 2019
Received in revised form 29 January 2020
Accepted 4 Febraury 2020
Available online xxx

Keywords
Three-leaf walls
Brick masonry
Interface
Compression tests
FEM simulation
Experimental tests

ABSTRACT

Three-leaf brick masonry wall is a typical technique in historical buildings.Sensitivity of three-leaf brick masonry wall to core mechanical characteristics and interface between layers is studied by reference to an experimental campaign.Experimental activities were performed on three-leaf masonry panel under compressive loads and is used to identify mechanical characteristic of three-leaf masonry wall and calibrate a 2D plain strain model (without and with interfaces between layers) for cross section of panel.A parametric analysis on inner core and interface between layers mechanical characteristic sensitivity is proposed.Numerical modeling results are presented and discussed in comparison with experimental data.

1. Introduction

Multiple layers often constitute most historical masonry buildings, realized by brick or stone block. A widespread multi-layer typology is the three-leaf brick masonry wall, which presents two external brick leaves and one inner core consisting of incoherent materials, with large presence of voids.

The behavior of multi-layer masonry structure is very difficult to investigate and its interpretation remains a challenge. A reason is in the non-linear and no tension masonry behavior which tends to brittle failure mechanisms, furthermore the multiple leaf walls presents a more complex mechanical behavior, with combined collapse mechanisms.

The literature is somehow missing and confined to laboratory experimental campaign of small dimensional panel [1–4]. Strengthened three-leaf stone masonry walls were analyzed by Silva et al. [5], Valluzzi et al. [6] and Vintzileou [7]. Numerical models were proposed by Milani [8,9] Aldreghetti et al. [10], Casolo & Milani. [11] and Silva et al. [12]. Contact surfaces in masonry modeling is also proposed in literature by adopting interfaces mortar joints and internal block [13]. Binda et al. [14] developed a theoretical model to predict the failure load on three-leaf masonry with the presence of stiff transversal elements to better distribute the vertical loads along leaves. Ramalho et al. [15] performed numerical analysis assuming a purely frictional Coulomb's law at the interface between the leaves to demonstrate that the interfacial cohesion between leaves could not be neglected. In a previous work, Pina-Henriques et al. [16] proposed a multi-surface interface model and set contact relationships between the inner core and the external leaves to describe the internal load distribution in a multi-leaf masonry.

In this paper, the experimental results are given for three-leaf masonry walls, realized at Laboratory of strength of materials IUAV (LabSCo), under compression load. The attention is focused on structural identification of multi-leaf masonry walls with a two-fold aim: calibrate numerical model and verify the reliability of related numerical simulations.

The proposed model is a first step modeling, referred to the cross section of masonry walls. Hence, a continuous 2D plane strain model is adopted by modeling the interface problem between the layers, i.e. contact relationships between the inner core and the external leaves and sensitivity to inner core mechanical characteristics. An interface model has been developed to reproduce the internal load distribution in a multi-leaf masonry under compression and results are evaluated with reference to experimental data obtained by tests carried out at LabSCo.

Hence the following sensitivity analyses are proposed:

- Sensitivity to core stiffness with reference to tested masonry panel;
- Sensitivity to interface model between external layers and core taking as reference the tested masonry panel;

* Corresponding author.
E-mail addresses: decarvalho@iuav.it (C.B. de Carvalho Bello); gboscato@iuav.it (G. Boscato); meroi@iuav.it (E. Meroi); cecchi@iuav.it (A. Cecchi)

https://doi.org/10.1016/j.conbuildmat.2020.118356
0950-0618/© 2020.

The aim is to develop a suitable approach to predict the performance of historical masonry walls by FEM simulation.

The paper is structured as follows. In Section 2 mechanical characteristic of materials and geometric description of masonry specimen are reported until to building phase of masonry realization. The test set up is exposed and experimental results are shown in terms of force versus displacement graphs. Section 3 is devoted to formulate FE model. A 2 D plain strain model is adopted for the panel cross section which represents the behavior of the three leaf masonry as a whole. To simulate three leaf masonry behavior, two model are proposed:

i. in the former, inner core and external layers are modeled as non-linear smeared cracked material with different stiffness to represent the random composition of inner core with reference to structure of external layers;
ii. in the latter, an interface model is implemented to allow local detachment between layers.

Section 4 carries on sensitivity analyses to several parameters of models (i) and (ii). Hence, calibration of models and comparison of models are proposed with reference to experimental results.

2. Masonry specimens

Masonry multi-leaf specimens were built with the following dimensions 142 × 144x38 cm^3, made of 22 brick layers, bed and head joint mortar 10 cm thick (see Fig. 1). Masonry panel specimens are manufactured with standard clay bricks for external layers (Danesi DM 116). The same mortar characteristics have been used for layers, joints and infills and they have been chosen in order to simulate a historical one with very low shear strength (Tassullo 14,303 CP/5).

The infill was realized with brick potsherds and mortar Tassullo CP/5 for 2/3 of the whole volume, while only bricks potsherds have been used to simulate the case of damaged infill conditions, in the last third, centrally placed with vertical reference.

Preliminary laboratory tests were performed on masonry constituents (bricks and mortar), in order to determine the mechanical properties to be adopted in FE models.

The mortar mechanical characteristics were determined by testing prisms (16 × 4 × 4 cm^3) after almost thirty days of air curing in accordance to the UNI EN 1015-11 standards [17]. Mean values were evaluated for flexural and compressive strength as 0.33 MPa and 1.16 MPa respectively. Mortar elastic modulus was evaluated as 800 Mpa, the secant value of the stress-strain curves obtained from compression tests at 60% of the peak stress.

Brick samples were tested in compression in accordance with UNI EN 772-1 [18]. Specimens allowed to determine a mean elastic modulus value equal to 4100 MPa. The shear strength was determined on nine specimens, without pre-compression, prepared in accordance to EN 1052e3 [19], with a mean value equal to 0.187 MPa.

Mechanical characteristics of brick and mortar are reported in Table 1.

In Fig. 1a and b, a geometric description is given for panels. In Fig. 1c, a detailed image is reported for construction phase. Simple compression tests were performed. To ensure the infill integrity, two masonry layers were built respectively at the bottom and at the top sites of each wall, with cement mortar horizontal layers reinforced by a steel textile net.

In addition, to favor a uniform load distribution under compression tests, panels have been refinished by cement mortar at bottom and top sites.

Three specimens (D1, D2 and D3 in the following) were simply compressed by a universal testing machine with a load capacity of 6000 kN, in displacement controlled conditions at a rate of 0.3 mm/min. The testing set-up included: six digital transducers, placed on both sides and connected to an electronic acquisition device; four vertical transducers with base length l_v = 30 cm and two horizontal ones with base length l_h = 42 cm. Fig. 2 reports the experimental load-displacement curves.

Fig. 3a shows testing set up and Fig. 3b, c and d the brittle failure mode with expected crack pattern along compression direction [20,21]. Crack pattern shown in Fig. 3c evidences load transfer on the top and bottom of specimen, characterized by a boundary effect that causes external layer detachment.

3. FE model

The masonry three-leaf panel is modeled by a continuous FE model. In this step, the section of panel is modeled in 2D plane strain conditions. We assume that a cross section (two external layers with regular texture and an internal incoherent core) is representative of the behavior of panel as a whole and the multi-purpose Diana code is used.

The two masonry external layers are built by brick arranged in a regular manner with mortar joint interposed.

The previous compression tests provided the evaluation of elastic modulus value of masonry specimens. Although, an estimation of each masonry layer (external leafs and inner core) is needed to perform the following FE simulations. A continuum equivalent orthotropic model for external masonry layers is then obtained, in linear field, through a homogenization procedure [22,23].

Young's modulus values obtained by experimental tests (reported in Table 1) are E_b = 4100 MPa and E_m = 800 MPa, respectively for brick and mortar, while the same Poisson's ratio is assumed ν = 0.15. In Fig. 4, standard homogenization boundary conditions are reported as applied to representative elementary volume (REV). The reference system x_1, x_2, x_3 is assumed, where x_1 is the in-layer-

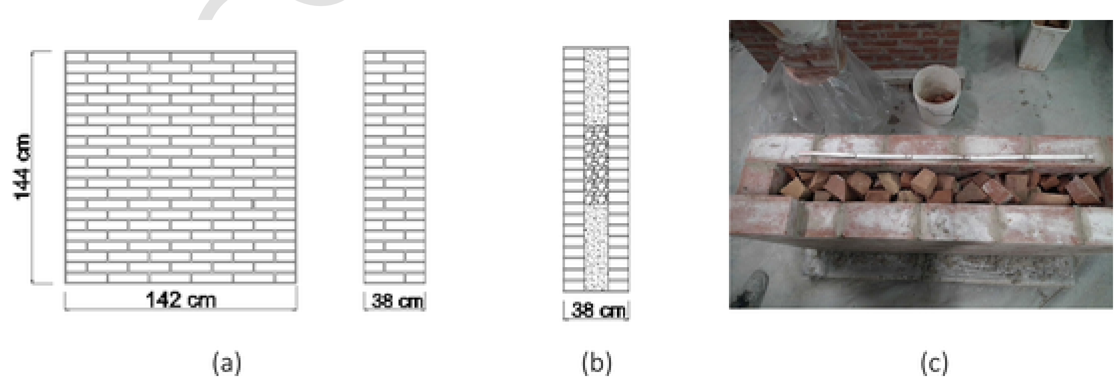

Fig. 1. Three-leaf masonry panels: front and left view (a), section (b) and under construction (c).

Table 1
Masonry constituents mechanical properties.

Mechanical parameters		Brick	Mortar
Compressive strength	[MPa]	–	1.16
Flexural strength		–	0.33
Elastic modulus		4100	800
shear strength		0.187	–

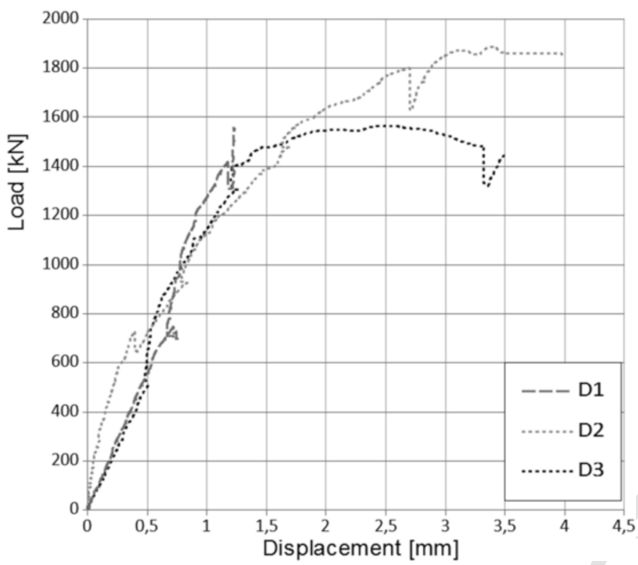

Fig. 2. Compression tests results: load-displacement graph.

plane horizontal axis, x_2 is the in-layer-plane vertical axis and x_3 is the axis along the layer thickness.

The following Table 2 shows homogenized elastic moduli for the external layer.

As masonry is considered as a composite homogeneous orthotropic material, the elastic homogenized modulus used in numerical simulation is in plane layer vertical Young's modulus $E_{22} = E_{ext} = 3063$ MPa and in plane layer vertical Poisson's ratio $\nu_{12} = 0.248$; the incoherent material of the inner core is simulated as a low stiffness elastic material with Young's modulus E_{core} equal to 90% of the is in plane layer vertical Young's modulus of external masonry and Poisson's ratio $\nu = 0.248$.

The fracture energy value (Gc) is evaluated in accordance with the Model Code 90 [24]. The code suggests for a masonry with compressive strength (f_c) lower than 12 MPa, the formulation $G_c = d{\cdot}f_c$, (where d = 1.6 mm). The tensile strength (f_t) and relative fracture energy (G_t) for masonry structures, in accordance with the experimental work performed by Van der Pluijim [25] within the following ranges: f_t = (0.1–0.2) [MPa] and G_t = (5–20) [N/m]. All mechanical properties of external layers and inner core are reported in Table 3; Fig. 5 reports constitutive relationships assumed in tension and compression.

Elastic brittle softening is assumed in tension and elastic softening parabolic behavior in compression, where h is the mesh element length [26].

All layers are modeled by 8-noded quadrilateral isoparametric elements according to Fig. 6.

Two different models are adopted: in the former, the three layers have only different mechanical characteristics from external layers and inner core; in the latter, 6-noded interface line elements are introduced between the inner core and the external leaves, with inelastic properties.

In this second model, vertical interfaces between external layers and inner core and horizontal interfaces at the top and bottom of the core are introduced in the formulation (see Fig. 7b). Mechanical characteristic of interfaces is showed in Fig. 7a. In a local reference system, stiffness orthogonal to interface is named k_n and stiffness parallel to interface k_s. It must be noted that different values are assumed for stiffness to simulate different contact condition between layers, being $K_n, K_s = 10^{-2}$ for nearly complete layers detachment and Kn,Ks = 10^2 for perfect continuity between layers. For interfaces, f_t is tension resistance and G_t is fracture energy in tension.

Hence the constitutive function of interface links stress to the Δu jump of displacement field, which is assumed as strain measure, between stiffness k_n orthogonal and k_s parallel to interface in a local reference system for interface. As shown in Fig. 8, tensile strength is used to simulate non-linear brittle behavior.

4. Sensitivity analyses

To calibrate numerical models, two sensitivity parametric analyses has been carried on:

- Sensitivity to stiffness of internal core.
- Sensitivity to stiffness of interfaces between layers.

This second analysis takes into account the model of interface at both lateral and top and bottom sites.

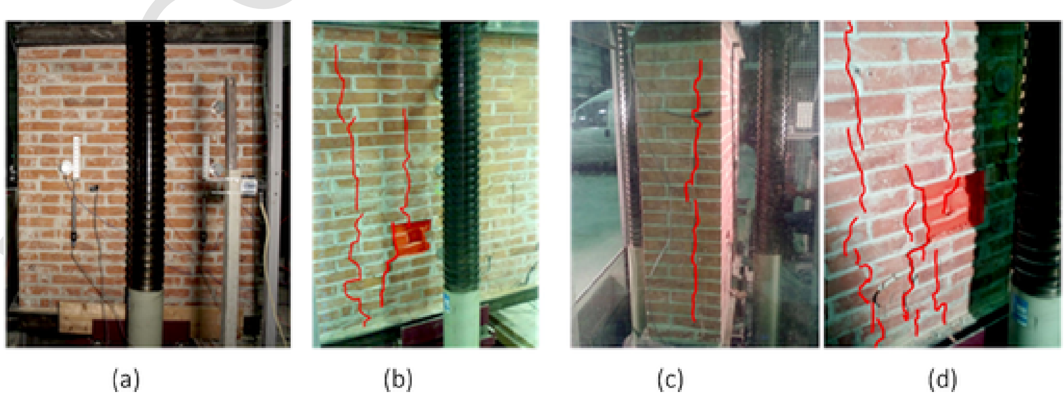

Fig. 3. Compression tests on three-leaf panels: crack patterns.

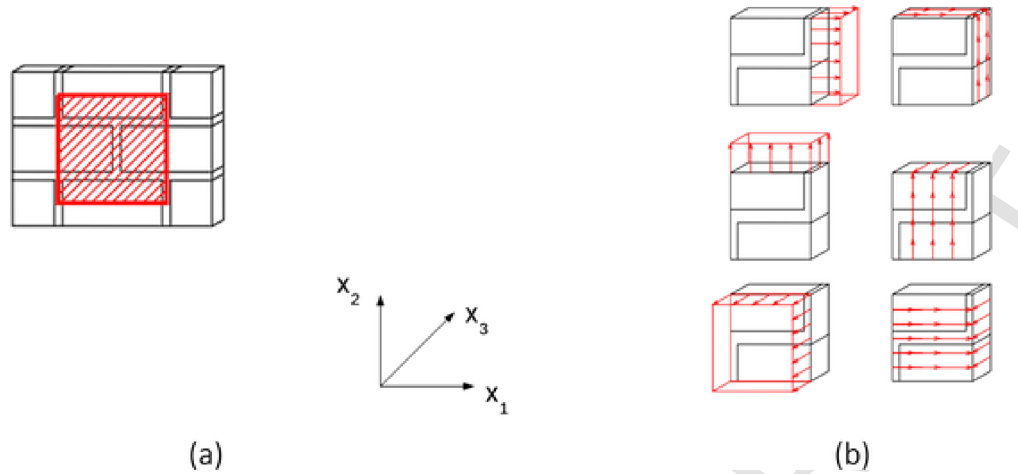

Fig. 4. Representative Element of Volume – REV (a) and periodic boundary conditions (b).

Table 2
Young modulus homogenized values for the external layer.

External masonry walls		
Young's modulus [MPa]	Shear modulus [MPa]	Poisson's Coefficients [MPa]
$E_{11} = 3450$	$G_{12} = 765$	$\nu_{12} = 0.220$
$E_{22} = 3063$	$G_{23} = 782$	$\nu_{12} = 0.248$
$E_{33} = 3560$	$G_{31} = 933$	$\nu_{12} = 0.210$

Table 3
Masonry mechanical properties.

Mechanical properties			External layer	Inner core
Young's modulus	E	[MPa]	3063	2756
Poisson's Coefficient	ν	–	0.248	0.248
Tensile strength	F_t	[MPa]	0.33	0.23
Fracture energy in tension	G_t	[N/mm]	0.02	0.02
Compressive strength	F_c	[MPa]	3.40	3.06
Fracture energy in compression	G_c	[N/mm]	5.45	4.90

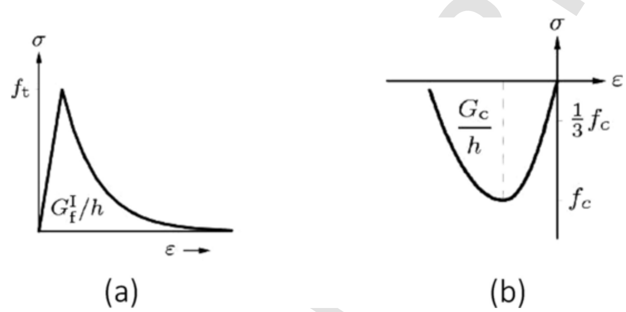

Fig. 5. Material constitutive law: a) Tension behavior; b) Compression behavior [26].

4.1. Sensitivity to inner core stiffness

In this section a parametric analysis of inner core stiffness has been performed. As reported in Table 4, the external layer mechanical characteristics are assumed constant, with varying mechanical

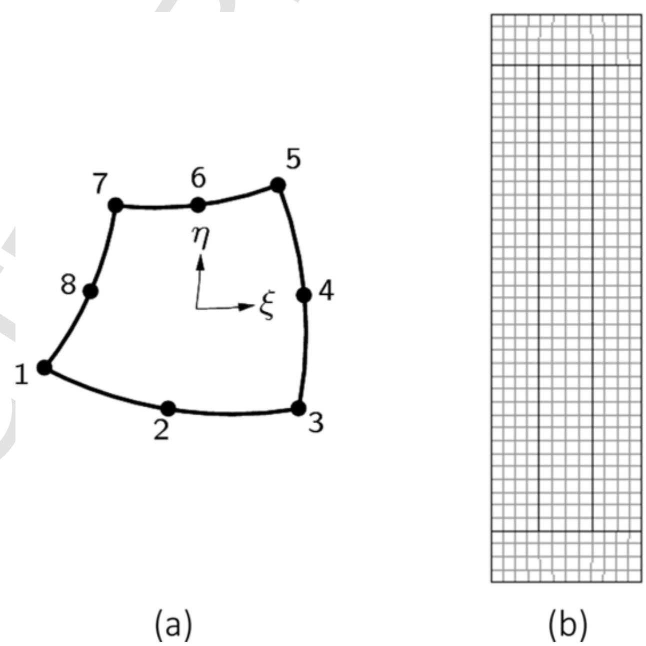

Fig. 6. Finite element adopted (a) [26] and panel 2D discretization.

characteristics of inner core. Three cases are proposed:

- full core with $E_{core} = E_{ext}$, where a homogeneous distribution is assumed for material characteristics;
- inner core with $E_{core} = 90\%\ E_{ext}$;
- low core with $E_{core} = 50\%\ E_{ext}$.

A pushover analysis has been performed to verify sensitivity to internal core stiffness.

All models – inner, full and low core– are compared with the results of compressive tests (see Fig. 9). With reference to the experimental scale of panel, pushover results suggest that the overall mechanical response is not deeply affected by core material properties. In all FE models, the peak panels resistance is very close with experimental values (Table 5).

In comparison with full core (FC) model, the relative difference between corresponding peak load of inner core (IC) model is 3.9%, while for low core (LC), the same decrement is evaluated.

Moreover, at the imposed displacement of 1 mm, for IC model the percentage decrement in tangential stiffness (with reference to

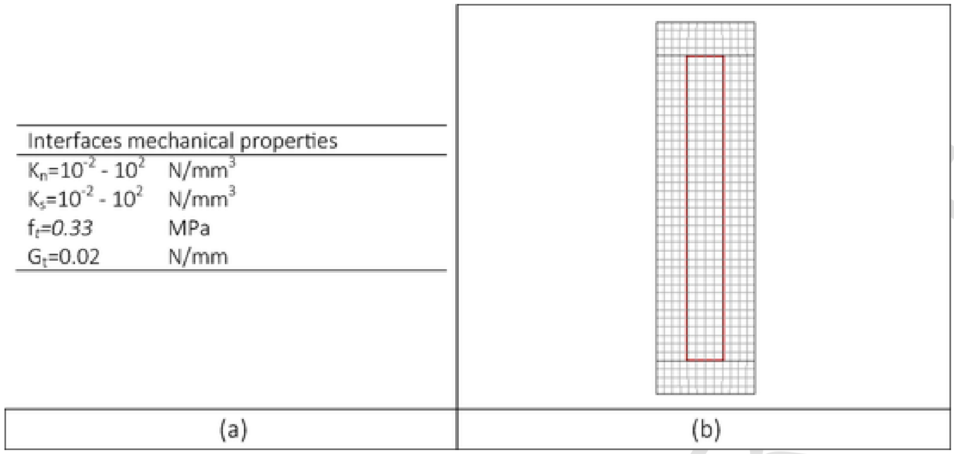

Fig. 7. Mechanical properties of interfaces (a) and FEM discretization (b).

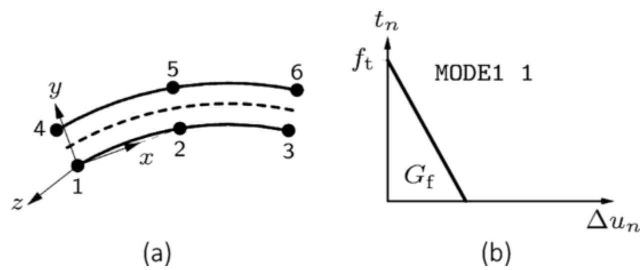

Fig. 8. Geometric description of interface element (a) and constitutive function of interface (b) [26].

Table 4
FE models mechanical properties.

Mechanical parameters			External layer	Inner core	Full core	Low core
Young's modulus	E	[MPa]	3063	2756	3063	1532
Poisson's coefficient	ν	ν	0.248	0.248	0.248	0.248
Tensile strength	F_t	[MPa]	0.33	0.23	0.33	0.17
Fracture energy in tension	G_t	[N/mm]	0.02	0.02	0.02	0.02
Compressive strength	F_c	[MPa]	3.40	3.06	3.40	1.70
Fracture energy in compression	G_c	[N/mm]	5.45	4.90	5.45	2.72

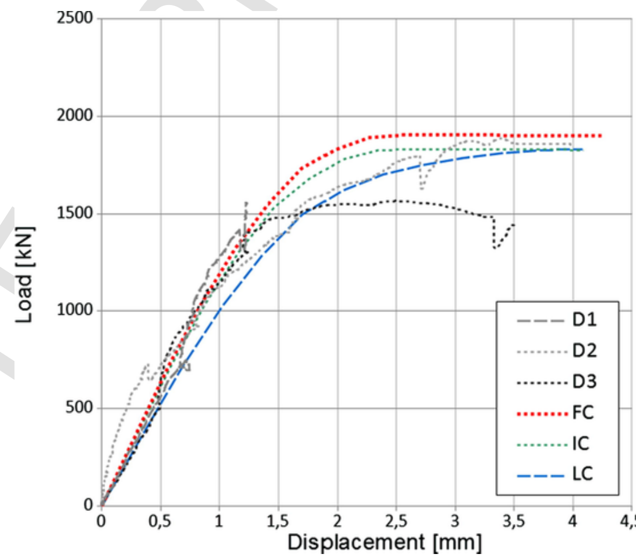

Fig. 9. FE models and compression tests results: load-displacement curves.

Table 5
FE models: internal core sensitivity analyses.

	Peak load [kN]	Displacement at Peak load [mm]	Tangential Stiffness [kN/mm]
FC	1905	2.83	1166
	–	–	–
IC	1832	2.63	1118
	3.9%	*7.0%*	*4.1%*
LC	1832	4.08	1001
	3.9%	*44.3%*	*14.1%*

full core result) is 4.1%, while it is 14.1% for low core (LC) model. Hence, the response of the model with this specimen dimension can be considered poorly sensible to the stiffness of internal core in the range of values considered (Table 6).

Fig. 10 shows the sensitivity of external layer with different inner core stiffness: the ratio between vertical stress value in external layer and inner core is correspondent to the elastic modulus inner core ratio: 90% in IC and 50% in LC model.

4.2. Sensitivity to interface characteristics between layers

At this stage, continuity assumption is discussed and further parametric analyses are presented to investigate model sensitivity to interface between inner core and external leafs.

Starting from previous experimentation and with reference to full core (FC) condition (see section 4.1), since internal core stiffness seems not to significantly affect the results, the specific interface contribution is evaluated. The analysis is performed in more steps, with the aim to separately evaluate the effect of lateral interfaces between layers only and also with top and bottom interface elements included.

In the case with only interfaces between leafs, Fig. 11a shows vertical load versus displacement curves for different lateral interface stiffness values; deformed mesh configurations are given for $k_n = k_s = 10^{-2}$N/mm^3 in Fig. 11b, named *full core lateral interface case* (FCLI$_a$) and $k_n = k_s = 10^2$N/mm^3, named *full core lateral interface case b* (FCLI$_b$) in Fig. 11c.

Table 6
FE models: interfaces sensitivity analyses.

	Peak load [kN]	Displacement at Peak load [mm]	Tangential Stiffness [kN/mm]
FC	1905	2.83	1166
	–	–	–
$FCLI_a$	1912	2.87	1150
	0.4%	*1.6%*	*1.3%*
$FCLI_b$	1912	2.86	1152
	0.4%	*1.3%*	*1.2%*
$FCHI_a$	1499	1.94	994
	21.3%	*31.5%*	*14.8%*
$FCHI_b$	1912	2.86	1152
	0.4%	*1.3%*	*1.2%*
$FCFI_a$	1247	11.10	718
	34.5%	*292.6%*	*38.5%*
$FCFI_b$	1912	2.86	1152
	0.4%	*1.3%*	*1.2%*

In details, for both cases FCLI, the relative percentage increment between corresponding peak load in the previous full core case FC and FCLI result is 0.4%. Moreover, the percentage stiffness reduction (evaluated for 1 mm displacement) is 1.3% for $FCLI_a$, and 1.2% for $FCLI_b$.

It can be pointed out that the vertical displacement percentage increment is 1.6% for $FCLI_a$ and 1.3% for $FCLI_b$.

Then, only horizontal interfaces at top and bottom core limits are introduced. Fig. 12a shows vertical load versus displacement curves for different interface stiffness values; deformed mesh configurations are given for $k_n = k_s = 10^{-2}$N/mm^3 named *full core horizontal interface case a* ($FCHI_a$) (Fig. 12b) and $k_n = k_s = 10^2$N/mm^3 named *full core horizontal interface case b* ($FCHI_b$) respectively (Fig. 12c).

In details, the relative percentage decrement between corresponding peak load in the previous full core case FC and $FCHI_a$ is 21.3%, while for $FCHI_b$ a relative percentage increment of 0.4% is obtained, the same achieved with lateral interfaces.

Moreover, the percentage stiffness reduction (evaluated at 1 mm displacement) is 14.8% for $FCHI_a$, and 1.2% for $FCHI_b$, equal to vertical interfaces cases $FCLI_b$.

It can be pointed out that the vertical displacement percentage increment is 31.5% for $FCHI_a$ and 1.3% for $FCHI_b$.

Furthermore, the sensitivity to both vertical and horizontal interfaces are proposed.

Fig. 13a shows load versus displacement curves for different interface stiffness values. It can be noted a significant difference in terms of displacements with the different interface stiffness; deformed mesh configurations are given for *case* named *full core full interface a* ($FCFI_a$) with $k_n = k_s = 10^{-2}$N/mm^3 (Fig. 13b) and for *case* named *full core full interface b* ($FCFI_b$) with $k_n = k_s = 10^2$N/mm^3 (Fig. 13c).

In details, the relative percentage decrement between corresponding peak load in the previous full core case FC and $FCFI_a$ is 34.5%; while for $FCFI_b$ relative percentage increment of 0.4% is obtained, the same achieved with other cases with higher stiffness values.

Moreover, the percentage stiffness reduction (evaluated at 1 mm displacement) is 38.5% for $FCFI_a$, and 1.2% for $FCFI_b$, equal to other cases with higher stiffness values.

In addition, it can be noted that the vertical displacement percentage increment is 292.6% for $FCFI_a$ and 1.3% for $FCFI_b$, the same value obtained in previous cases with higher stiffness interface values.

Table 3 reports all numerical simulations results about interface sensitivity.

Once sensitivity analysis was made, the FCFI model has been calibrated with experimental results (D2 and D3). For lateral interfaces, the stiffness considered are k_n, $k_s = 10^2$N/mm^3. The horizontal interfaces stiffness assumes different values, depending on the considered sample. For the sample D3, the stiffness values are $k_n = 10^{-2}$N/mm^3 and $k_s = 10^2$N/mm^3: $FCFI_3$ model. Considering D2 curve, $FCFI_2$ model assumes $k_n = k_s = 10^2$N/mm^3. In Fig. 13, pushover plots in comparison of experimental results are reported (Fig. 14).

Fig. 15 shows the dependence of vertical stress in external layer considering different contact conditions (interfaces) between layers. The same stiffness ratio is kept between external layers and inner core. In a model calibration based on interfaces characteristics, different nonlinear responses of three-leaf panels can be obtained in terms of stiffness, peak load, and post-damage softening.

5. Conclusions

The present analyses are relative to a sensitivity investigation of inner core mechanical characteristics, and interface formulations between layers. The FE model has been calibrated by reference to experimental testing at LabSCo on three-leaf masonry panel subjected to compressive load.

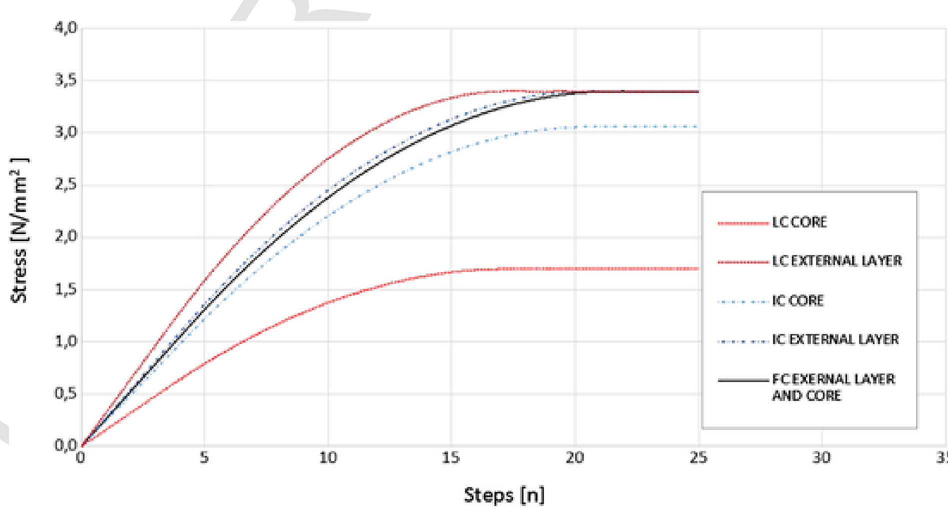

Fig. 10. FE models without interfaces: stress-step load increment curves.

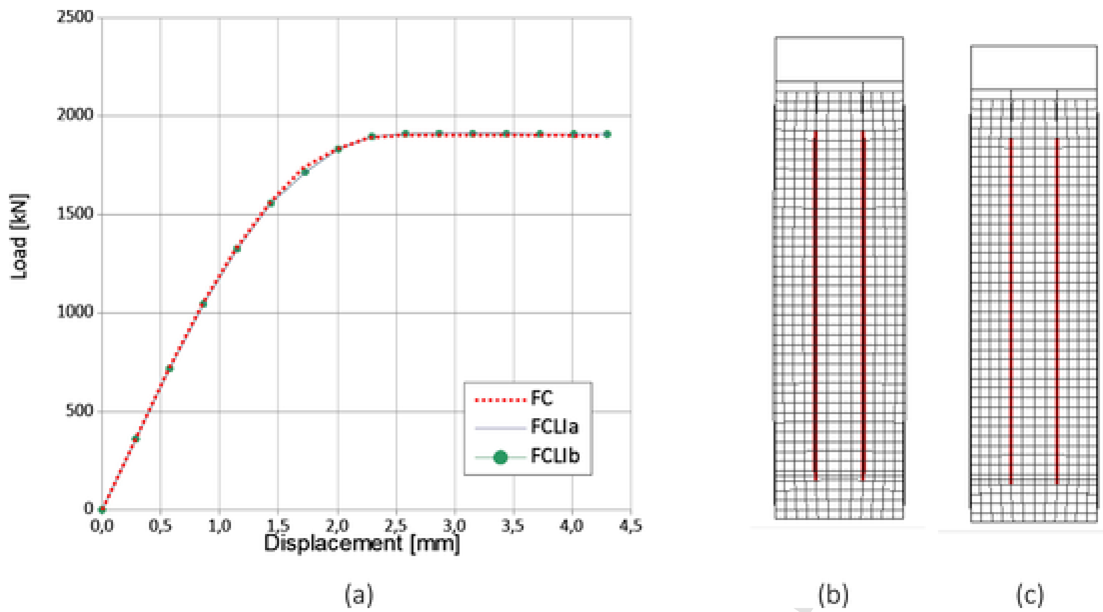

Fig. 11. FEM with lateral interfaces between layers: load-displacement graph (a) and deformed mesh of lower (a) and upper (b) bound interface stiffness.

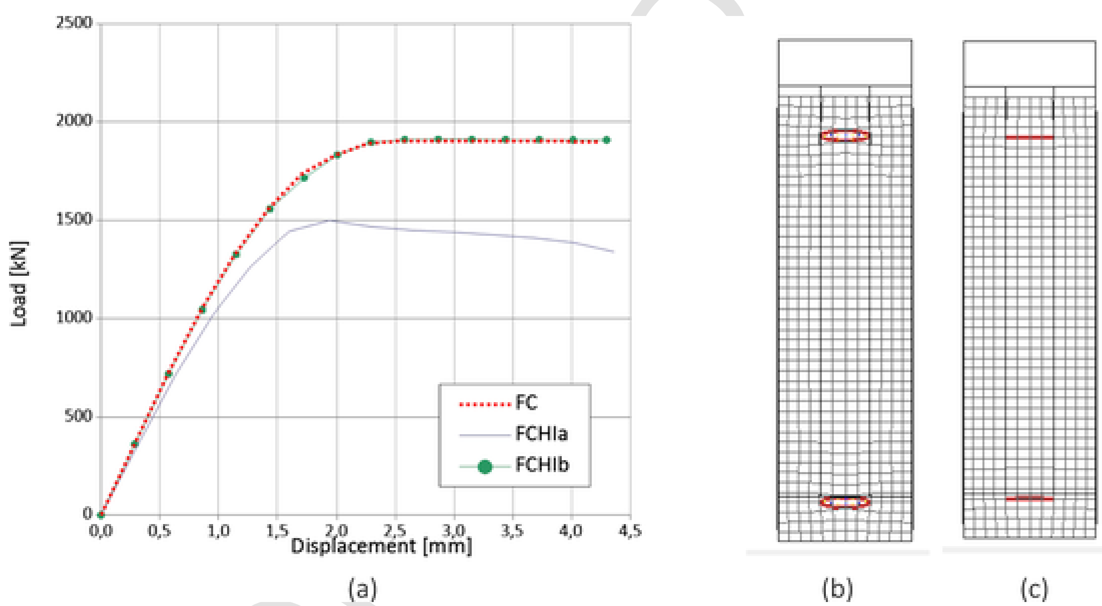

Fig. 12. FEM with horizontal interfaces between layers: load-displacement graph (a) and deformed mesh of lower (a) and upper (b) bound interface stiffness.

The panel cross section is modeled by a 2D plain strain continuous model, firstly with continuity assumption and then with interface elements between inner core and bricks: fitting of experimental results have been obtained after mechanical properties identification.

This parametric analysis shows:

- in a reasonable range of values, inner core mechanical characteristic does not influence mechanical behavior of this three leaf structure;
- interface between layers influences mechanical characteristics. In detail, lateral interfaces between leafs show a negligible influence on peak load, tangential Stiffness and vertical displacements;
- horizontal interfaces at the top and bottom of inner core show a considerable influence on peak load and vertical displacements of masonry panels;
- full interfaces (all around the inner core) show that the orthogonal stiffness of horizontal interfaces are the most important parameter to set for the calibration of compression tests;
- with reference to experimental tests of three-leaf panels, interfaces are used in the FE model to simulate the detachment observed between different layers. They can be calibrated to simulate this behavior and related failure modes.

Hence for the specimen dimension that are limited with reference to effective structures, interfaces between layers seems to represent a proper method to individuate panel lower and upper stiffness limits and to calibrate numerical models in accordance with experimental results. The present results constitute the first step of a work in progress. Further experimental tests will be performed considering different masonry sizes to evaluate size effect sensibility.

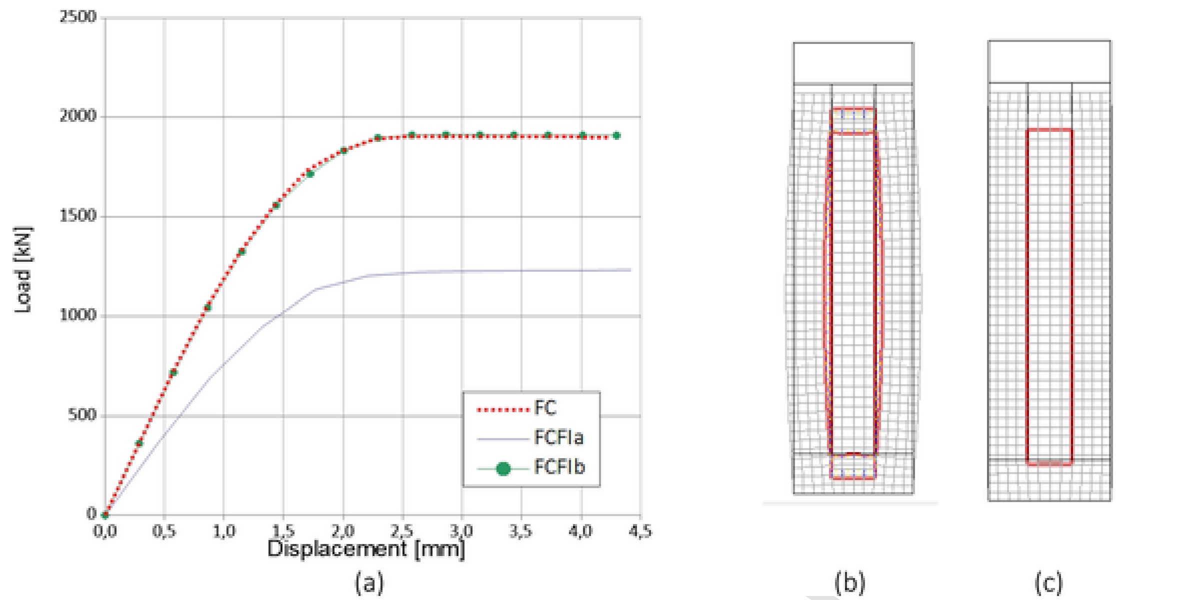

Fig. 13. FEM with vertical and horizontal interfaces between layers: load-displacement graph (a) and deformed mesh of lower (a) and upper (b) bound interface stiffness.

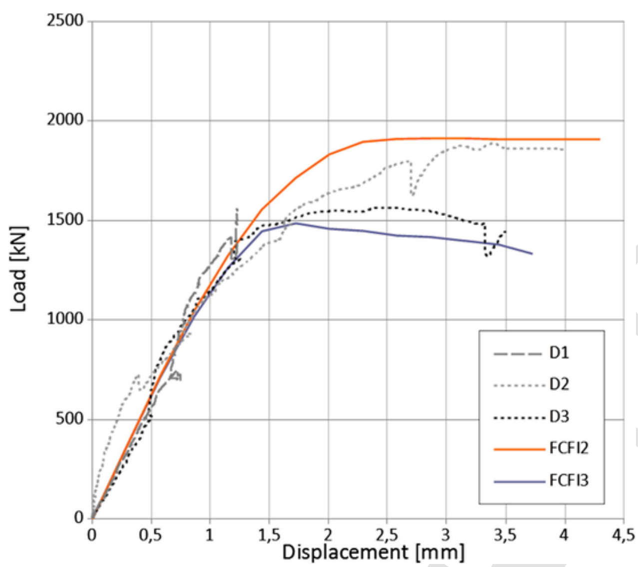

Fig. 14. FE models pushover results: calibration of FCFI model with experimental results.

Declaration of Competing Interest

The authors declare that they have no known competing financial interests or personal relationships that could have appeared to influence the work reported in this paper.

Acknowledgments

The authors acknowledge the Laboratory of strength of materials of the University IUAV of Venice (Labsco) for the support given at these experimental tests. This work was partly financed by the research project PRIN 2017 (under grant 2017HFPKZY_002, project "*Modelling of constitutive laws for traditional and innovative building materials*").

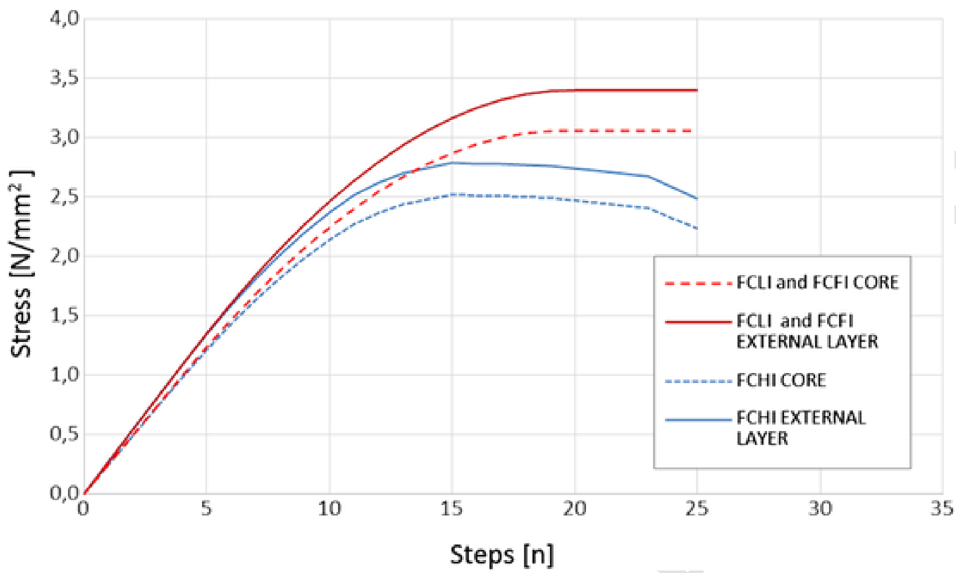

Fig. 15. FE models with interfaces: stress-step load increment curves.

References

[1] C.B. de Carvalho Bello, A. Cecchi, E. Meroi, Three leaf masonry walls: the scale factor, Proceedings of EUROMECH COLLOQUIUM 584, 2016.
[2] D.V. Oliveira, P.B. Lourenço, E. Garbin, M.R. Valluzzi, C. Modena, Experimental investigation on the structural behaviour and strengthening of three-leaf stone masonry walls, Proceedings of Structural Analysis of Historical Constructions, New Delhi, 2006.
[3] M. Ramalho, A. Taliercio, A. Anzani, L. Binda, E. Papa, Experimental and numerical study of multi-leaf masonry walls, WIT Trans. Built Environ. (2005) 333–342.
[4] D.V. Oliveira, R.A. Silva, E. Garbin, P.B. Lourenço, Strengthening of three-leaf stone masonry walls: an experimental research, Mater Struct. 45 (2012) 1259–1276.
[5] B. Silva, M. Dalla Benetta, F. Da Porto, C. Modena, Experimental assessment of in plane behaviour of three-leaf stone masonry walls, Constr Build Mater. 53 (2014) 149–161.
[6] M.R. Valluzzi, F. Da Porto, C. Modena, Behavior and modeling of strengthened three-leaf stone masonry walls, Mater Structures/Materiaux Constr. 37 (267) (2004) 184–192.
[7] E. Vintzileou, Three-leaf masonry in compression, before and after grouting: a review of literature, Int. J. Archit. Herit. 5 (2011) 513–538 4e5.
[8] G. Milani, 3D upper bound limit analysis of multi-leaf masonry walls, Int. J. Mech. Sci. 50 (4) (2008) 817–836.
[9] G. Milani, 3D FE limit analysis model for multi-layer masonry structures reinforced with FRP strips, Int. J. Mech. Sci. 52 (6) (2010) 784–803.
[10] I. Aldreghetti, D. Baraldi, G. Boscato, A. Cecchi, L. Massaria, M. Pavlovic, et al., Multi-leaf masonry walls with full, damaged and consolidated infill: experimental and numerical analyses, Key. Eng. Mater. 747 (2017) 488–495.
[11] S. Casolo, G. Milani, Simplified out-of-plane modelling of three-leaf masonry walls accounting for the material texture, Construction and Building Materials, Special Section on Recycling Wastes for Use as, Constr. Mater. 40 (2013) 330–351.
[12] B.Q. Silva, A. Pappas, J.M. Guedes, F. da Porto, C. Modena, Numerical analysis of the in-plane behaviour of three-leaf stone masonry panels consolidated with grout injection, Bull Earthquake Eng 15 (2017) 357–383.
[13] P.B. Lourenço, J.G. Rots, A multi-surface interface model for the analysis of masonry structures, ASCE J. Eng. Mech. 123 (7) (1997) 660–668.
[14] L. Binda, J. Pina-Henriques, A. Anzani, A. Fontana, P.B. Lourenço, A contribution for the understanding of load-transfer mechanisms in multi-leaf masonry walls: testing and modelling, Eng. Struct. 28 (8) (2006) 1132–1148.
[15] M.A. Ramalho, A. Taliercio, A. Anzani, L. Binda, E. Papa, A numerical model for the description of the nonlinear behaviour of multi-leaf masonry walls, Adv. Eng. Softw. 39 (4) (2008) 249–257.
[16] J. Pina-Henriques, P.B. Lourenço, L. Binda, A. Anzani, Testing and modelling of multi-leaf masonry walls under shear and compression, Proceedings of IV International Seminar on Structure Analysis of Historic Constructions, Padova, 2004, pp. 299–310.
[17] UNI EN 1015-11: 2007: Methods of test for mortar for masonry. Part 11: Determination of flexural and compressive strength of hardened mortar (in Italian). Ente Italiano di Unificazione: Milano Mar. 2007.
[18] UNI EN 772-1: 2011: Methods of test for masonry units. Part 1: Determination of compressive strength (in Italian). Ente Italiano di Unificazione: Milano Jun. 2011.
[19] EN1052-3:2002/A1:2007. 2007. Methods of test for masonry. Part 3: Determination of initial shear strength. Brussels (BE): CEN.
[20] R. Egermann, Experimental analysis of multiple leaf masonry wallets under vertical loading, Structural repair and maintenance of historical buildings II (1991) 197-208.
[21] A. Drei, A. Fontana, Influence of geometrical and material properties on multiple-leaf walls behaviour, 7 (2001).
[22] G. Boscato, E. Reccia, A. Cecchi, Non-destructive experimentation: Dynamic identification of multi-leaf masonry walls damaged and consolidated, Compos. B Eng. 133 (2018) 145–165.
[23] C.B. de Carvalho Bello, D. Baraldi, G. Boscato, A. Cecchi, E. Meroi, I. Aldreghetti, G. Costantini, L. Massaria, V. Scafuri, I. Tofani, Numerical and theoretical models for NFRCMstrengthened masonry, Mechanics of Masonry Structures strengthened with composite materials: Modeling, testing, design, monitoring, control, MuRiCo6, Bologna (2019).
[24] CEB-FIP Model Code 90 (Thomas Telford Ltd., UK, 1993).
[25] Pluijm RVD. Material properties of masonry and its components under tension and shear. In: Proceedings of 6th Canadian Masonry Symp. Saskatoon, June, 1992. p. 675–686.
[26] TNO DIANA, DIANA. DIsplacement method ANAlyser, release 9.4, User's Manual.